Experimental Research

INTERNATIONAL JOURNAL OF SURGERY

OPEN

Single dual-specific anti-PD-L1/TGF-β antibody synergizes with chemotherapy as neoadjuvant treatment for pancreatic ductal adenocarcinoma: a preclinical experimental study

Haoxiang Zhang, MD, PhD[a,b,c,d], Jiaoshun Chen, MD[a,d], Jianwei Bai, MD[a,d], Jing Zhang, MS[e], Shaoyi Huang, PhD[e], Liang Zeng, MS[e], Pengfei Zhou, MD, PhD[e], Qiang Shen[f], Tao Yin, MD, PhD[a,d,*]

Aims: Chemotherapy resistance is an important cause of neoadjuvant therapy failure in pancreatic ductal adenocarcinoma (PDAC). BiTP (anti-PD-L1/TGF-β bispecific antibody) is a single antibody that can simultaneously and dually target transforming growth factor-beta (TGF-β) and programmed cell death ligand 1 (PD-L1). We attempted in this study to investigate the efficacy of BiTP in combination with first-line chemotherapy in PDAC.

Methods: Preclinical assessments of BiTP plus gemcitabine and nab-paclitaxel were completed through a resectable KPC mouse model (C57BL/6J). Spectral flow cytometry, tissue section staining, enzyme-linked immunosorbent assays, Counting Kit-8, transwell, and Western blot assays were used to investigate the synergistic effects.

Results: BiTP combinatorial chemotherapy in neoadjuvant settings significantly downstaged PDAC tumors, enhanced survival, and had a higher resectability for mice with PDAC. BiTP was high affinity binding to targets and reverse chemotherapy resistance of PDAC cells. The combination overcame immune evasion through reprogramming tumor microenvironment via increasing penetration and function of T cells, natural killer cells, and dendritic cells and decreasing the function of immunosuppression-related cells as regulatory T cells, M2 macrophages, myeloid-derived suppressor cells, and cancer-associated fibroblasts.

Conclusion: Our results suggest that the BiTP combinatorial chemotherapy is a promising neoadjuvant therapy for PDAC.

Keywords: dual-specific antibody, immune checkpoint inhibitor, immune evasion, neoadjuvant chemoimmunotherapy, pancreatic ductal adenocarcinoma, programmed cell death ligand 1, transforming growth factor-β, tumor microenvironment

Introduction

Pancreatic ductal adenocarcinoma (PDAC) represents one of the leading causes of cancer-related death and is projected to become the second leading cause of cancer-related death by 2030[1]. With non-specific clinical symptoms, early diagnosis of PDAC is difficult, rendering most pancreatic cancer patients diagnosed with borderline either resectable (BR), locally advanced (LA), or metastatic stages. Currently, surgery remains the only hope for a cure for pancreatic cancer. Surgical resection is not recommended in patients with BR and LA lesions due to high morbidity, low rate of R0 resection, and high rate of early systemic recurrence. Only 15–20% of patients undergo radical surgical resection.

Neoadjuvant therapy has dramatically improved the prognosis of PDAC patients with LA and BR stage lesions over the past decade[2–5]. A growing body of evidence suggests that in addition to direct cytotoxic effects on cancer cells, neoadjuvant therapy can restore local antitumor immune response in PDAC[6–8].

[a]Department of Pancreatic Surgery, Union Hospital, Tongji Medical College, Huazhong University of Science and Technology, Wuhan, [b]Department of Hepatopancreatobiliary Surgery, Shengli Clinical Medical College of Fujian Medical University, Fuzhou, [c]Department of Hepatopancreatobiliary Surgery, Fujian Provincial Hospital, Fuzhou, [d]Sino-German Laboratory of Personalized Medicine for Pancreatic Cancer, Union Hospital, Tongji Medical College, Huazhong University of Science and Technology, Wuhan, [e]Wuhan YZY Biopharma Co., Ltd, Biolake, Wuhan, People's Republic of China and [f]Department of Interdisciplinary Oncology, Louisiana State University Health Sciences Center, New Orleans, LA, United States

Haoxiang Zhang and Jiaoshun Chen contributed equally to this work.

Sponsorships or competing interests that may be relevant to content are disclosed at the end of this article.

*Corresponding author. Address: No. 1277 Jiefang Avenue, Wuhan, Hubei 430022, People's Republic of China. Tel.: +860 278 535 1631. E-mail: ytwhun@hust.edu.cn (T. Yin).

International Journal of Surgery (2024) 110:2679–2691

Received 23 November 2023; Accepted 13 February 2024

Supplemental Digital Content is available for this article. Direct URL citations are provided in the HTML and PDF versions of this article on the journal's website, www.lww.com/international-journal-of-surgery.

Published online 14 March 2024

http://dx.doi.org/10.1097/JS9.0000000000001226

Preclinical studies have shown that neoadjuvant approaches enhance systemic immunity and more effectively eradicate residual metastasis[9,10].

Cancer immunotherapy has been transformed by immune checkpoint inhibitors (ICIs), which have significantly improved clinical outcomes in immunogenic cancers, such as melanoma, lung cancer, and prostate cancer. However, single-agent immunotherapies (anti-CTLA-4 and anti-PD-L1) are ineffective in treating PDAC[11–14]. This failure is likely due to the highly immunosuppressive tumor microenvironment (TME), which leads to immune evasion in PDAC. Transforming growth factor-beta (TGF-β) was found to play a pivotal role in resistance to ICIs because TGF-β is a major regulator of TME. TGF-β activation with peritumoral extracellular matrix-rich stromal formation is associated with PD-L1 resistance in cancer patients[14]. In advanced-stage cancers, TGF-β promotes distant metastasis, drug resistance, and immune escape[15–17]. In a recent study, we used the Check-BODY platform to design and construct bispecific antibodies that are able to dually and simultaneously block TGF-β and murine PD-L1 (YM101). These dual-targeting specific antibodies have displayed potent antitumor activity without observable toxicity in multiple mouse tumor models[18–20].

Combinatorial ICI therapy approaches with chemotherapy and/or radiotherapy are promising neoadjuvant therapies to improve resectability and survival of patients with LA and BR stage pancreatic cancer. Here, we investigated the bioactivity of our specific, dual-targeting TGF-β and PD-L1 (both human and murine) antibody (termed BiTP) and the antitumor activity of adjuvant and neoadjuvant BiTP plus chemotherapy (gemcitabine and nab-paclitaxel) in treating PDAC and exploring their underlying mechanisms of action.

HIGHLIGHTS

- BiTP is a single antibody that can simultaneously and dually target transforming growth factor-beta and programmed cell death 1 ligand 1.
- BiTP combinatorial chemotherapy significantly downstaged pancreatic ductal adenocarcinoma (PDAC) tumors.
- BiTP combinatorial chemotherapy is a promising neoadjuvant therapy for PDAC.
- The combination overcame immune evasion through reprogramming tumor microenvironment.

Materials and methods

Cell lines and antibodies

Human PDAC cell lines ASPC-1 (with Kras G12D mutation) and CFPAC-1 (with Kras G12V mutation) and human pancreatic ductal epithelial cell line HPDE6-C7 were obtained from China Center for the Conservation of Typical Cultures (CCTCC). Mouse PDAC cell lines LSL-Kras (+/G12D), LSL-Trp53 (+/R172H), and Pdx1-Cre (KPC; representing the Kras G12D mutation and Trp53 R172H mutation) were derived from the primary pancreatic tumor of a male KPC gene-edited mouse and kindly provided by Shanghai Cancer Center, Fudan University. After obtaining the KPC cell lines, we determined the mutation type by next-generation sequencing (NGS) performed by Biotech (Biotech Biotech, Shanghai, China). All cell lines were cultured in Dulbecco's modified Eagle's medium (DMEM; BasalMedia, Shanghai, China) containing 10% fetal bovine serum (FBS; Biological Industries, Kibbutz Beit-Haemek, Israel) and 1% penicillin/streptomycin (BasalMedia, Shanghai, China). The cells were incubated at 37°C with 5% CO_2. The absence of mycoplasma contamination was verified using MycoBlue Mycoplasma Detector (Vazyme, Nanjing, China). Therapeutic antibodies used in this work were purchased from YZY Biopharma, Wuhan, China (Supplementary Table 1, Supplemental Digital Content 1, http://links.lww.com/JS9/C71).

Determination of BiTP binding to TGF-β1/2/3 antigens and PD-L1 antigen

We coated 96-well enzyme-linked immunosorbent assay (ELISA) plates with 100 μl of TGF-β1 (Z03411, GenScript, New Jersey, USA), TGF-β2 (Genescript, Z03429), or TGF-β3 (Genescript, Z03430) antigen, and human PD-L1-7HIS antigen or mouse PD-L1 antigen at 2 μg/ml for incubation overnight at 4°C. The plates were sealed with phosphate-buffered saline (PBS; BasalMedia, Shanghai, China) containing 3% bovine serum albumin (BSA) (3% BSA-PBS) at 37°C for 2 h. Then, serial dilutions of therapeutic BiTP (Wuhan YZY Biopharma), therapeutic anti-PD-L1 antibody (atezolizumab, anti-PD-L1 antibody, Roche, Basel, Suisse), or therapeutic anti-TGF-β antibody (Wuhan YZY Biopharma, Wuhan, China) were added according to the experimental design. The plates were incubated at 37°C for 1 h. Mouse anti-human IgG Fc antibody [horseradish peroxidase (HRP) coupled] secondary antibody was added to the plate and incubated at 37°C for 1 h. Each plate was then colored with TMB substrate (Beyotime, P0209) and the reaction was terminated with a termination solution before the absorbance at OD450 nm was measured using an enzyme marker (Thermo Fisher Scientific, Massachusetts, USA).

Determination of competition of BiTP for binding of TGF-β1/2/3 with TGF-βRII and PD-L1 with PD-1

We coated 96-well ELISA plates with 100 μl of TGF-β1 (2 μg/ml), TGF-β2 (2 μg/ml), TGF-β3 (2 μg/ml) antigen, human PD-L1-7HIS antigen (10 μg/ml), or mouse PD-L1 antigen (2 μg/ml) for incubation overnight at 4°C. The plates were sealed with (3% BSA-PBS) at 37°C for 2 h. Then, 3 μg/ml of TGFBRII-6H or mouse PD-L1-Fc was added to plates in the presence or absence of serial dilutions of BiTP or anti-PD-L1 antibody or anti-TGF-β antibody. Then the plates were incubated at 37°C for 1 h. Secondary antibody was then added, followed by mouse anti-6×His HRP antibody or peroxidase-coupled streptavidin to the plates for incubation at 37°C for 1 h. The absorbance at OD450 nm was measured using an enzyme marker after plates were developed with TMB substrate and terminated with termination solution. The materials used in this study are listed in Supplementary Table 1 (Supplemental Digital Content 1, http://links.lww.com/JS9/C71).

Animal models

All *in vivo* animal experiments in this study followed the ethical standards of the Institutional Animal Care and Use Committee (IACUC) of Tongji Medical College, Huazhong University of

Science and Technology. Ethical approval for this study was provided on 1 January 2022 (IACUC Protocol number: 3044). This work has been reported in accordance with the ARRIVE guidelines, Supplemental Digital Content 2, http://links.lww.com/JS9/C72 (Animals in Research: Reporting In Vivo Experiments)[21]. Mouse euthanasia procedures were performed in accordance with the American Veterinary Medical Association Guidelines for Euthanasia of Animals to minimize animal pain and suffering (https://www.avma.org/sites/default/files/2020-02/Guidelineson-Euthanasia-2020.pdf).

Eight-week-old male C57BL/6J mice were purchased from Beijing Weitong Lihua Experimental Animal Technology Co., Ltd (Beijing, China) and bred under specific pathogen-free conditions in the laboratory animal center of Tongji Medical College, Huazhong University of Science and Technology (Wuhan, China).

Orthotopic tumor transplantation PDAC models (KPC) of immune-competent C57BL/6J mice

C57BL/6J mice ($n = 8$ each group) were anesthetized with an intraperitoneal (i.p.) injection of 1.25% tribromoethanol (Nanjing Aibei Biotechnology, 20 μl/g mouse). The fur was shaved in the left flank using an electric clipper and cleaned with a small vacuum. The region of the incision was sterilized with 75% alcohol. Matrigel (BD, Cat #354248) was kept at 0°C. KPC cells were fully resuspended in PBS and mounted with PBS/Matrigel in a 1:1 dilution (5×10^5 cells/20 μl). The tumor cell suspension (20 μl) was injected into the tail of the pancreas, which was exposed under the left-flank incision. The syringe needle was pulled out after the Matrigel solidified (20 s). The abdominal wall was sterilized with 75% alcohol again and closed in layers with a 7-0 silk suture.

Decisions about resectability status in PDAC murine models

To better characterize and reflect clinical progression scenarios of PDAC patients, by referring to the grading criteria for resectability of human pancreatic cancer tumors set in the National Comprehensive Cancer Network (NCCN) guidelines (https://www.nccn.org/professionals/physician_gls/pdf/pancreatic.pdf), we proprietarily established a mouse orthotopic pancreatic cancer tumor staging standard to evaluate the resectability and therapeutic effect (Supplementary Table 2, Supplemental Digital Content 1, http://links.lww.com/JS9/C71).

Therapeutic drug dosage and administration

In tumor-bearing mice, BiTP (13.3 mg/kg), anti-PD-L1 (10 mg/kg), or isotype control (10 mg/kg) was administered via i.p. injection in 0.1 ml saline with 0.005% Tween-80. Gemcitabine (50 mg/kg) and nab-paclitaxel (10 mg/kg) were administered with i.p. injection in 0.2 ml saline with 0.005% Tween-80. The exact dose and treatment schedules for each experiment are listed in the figure legends and schematics.

Distal pancreatectomy

C57BL/6J mice were anesthetized with i.p. injection of 1.25% tribromoethanol (20 μl/g). The fur in the surgical field was shaved and cleaned. The incision site was sterilized with 75% alcohol. A small abdominal incision (5 mm) was made in the left flank. Abdominal organs (intestine; stomach; liver; kidneys; pelvic, peritoneal, and retroperitoneal areas; or ascites) were examined for macroscopic metastases. Indications for surgery included successful modeling (tumors diameter reaching around 3 mm) and no distant metastasis or evidence of direct invasion of surrounding organs. The posterior pancreas space was dissociated from the body and tail of the pancreas, and the pedicle of the spleen was exposed. The body of the pancreas was clamped with microscopic tissue forceps, and the tail portion was cut off with a scalpel, with an intact tumor in the tail of the pancreas. The pancreatic stump was allowed to reach homeostasis using bipolar coagulation (Wuhan Spring Scenery Medical Instrument Co., Ltd, CHR-V). After ensuring no active bleeding in the abdominal cavity, the abdomen wall was sterilized with 75% alcohol again and closed in layers with a 7-0 silk suture.

Adjuvant therapy and neo-adjuvant therapy

One week after tumor cell inoculation, the tumors diameter reached around 5 mm (BR status), and the mice were randomly grouped into direct operation and neoadjuvant therapy groups. In the direct operation group, the tail of the pancreas (including the complete tumor and the surrounding normal pancreatic tissue over 2 mm) was directly removed by laparotomy, and chemotherapy or chemoimmunotherapy (BiTP plus chemotherapy) was performed after recovery (one week). In the neoadjuvant therapy group, chemotherapy or neoadjuvant chemoimmunotherapy (BiTP plus chemotherapy) was performed first. The remaining tumor tissue was surgically removed (including the complete tumor and the surrounding normal pancreatic tissue over 2 mm) when the course of neoadjuvant therapy ended. The mice could tolerate surgical resection (after the body weight returned to the level before neoadjuvant therapy). Owing to the limitations of our technical conditions, lymph node dissection could not be achieved during the surgery, which may be the reason for the death of the mice due to the potential tumor recurrence. For the animals that showed invasion of the surrounding organs and blood vessels during the operation, we judged the animals as being in the terminal stage and were euthanized because the combined excision of blood vessels and organs could not be performed. Mice that died intraoperatively or within 3 days after surgery were defined to have undergone a surgery-related death. Operative mortality (OM) was calculated as the number of surgery-related deaths divided by the total number of operations.

Tumor growth and survival

Tumor sizes (length × width) were measured every 5 days by palpation and small animal ultrasound (Xuzhou Ruishengchaoying Electronic Technology Co., Ltd). Tumor volume (mm^3) was calculated as follows: $1/2 \times \text{length} \times \text{width}^2$. The formula for relative tumor proliferation rate (T/C) was as follows: T_{TV} (the relative tumor volume of the treatment group)/C_{TV} (the relative tumor volume of the control group) × 100%. The tumor growth inhibition ratio (TGI, %) was calculated using the following formula: TGI (%) = 100% – T/C (%). Kaplan–Meier survival curves were generated to compare the percentage survival between different treatment groups. The significant difference in survival curves was analyzed with the log-rank (Mantel–Cox) test (Supplementary Table 3, Supplemental Digital Content 1, http://links.lww.com/JS9/C71).

Spectral flow cytometry

Tumors were minced and digested with collagenase B (1 mg/ml; Roche), hyaluronidase (0.5 mg/ml; Biosharp), and deoxyribonuclease I (0.1 mg/ml; Biosharp); and incubated in a thermostatic shaker (37°C with shaking at 100 rpm) for 1 h. Suspensions were filtered through 40 μm cell strainers. We examined the intratumoral infiltration of the most studied cell populations in pancreatic cancer through spectral flow cytometry, including antitumor immune-related cells, natural killer (NK) cells (NK-1.1$^+$ NK cells), effector NK cells (Gzmb$^+$, Perforin$^+$ NK cells), CD8 T cells (CD3$^+$ CD8$^+$ T cells), effector CD8$^+$ T cells (Gzmb$^+$, IFN-γ$^+$, Perforin$^+$, and Ki67$^+$ CD8 T cells), CD4 T cells (CD3$^+$ CD4$^+$ T cells), exhausted CD8 T cells (PD-1$^+$ CD8$^+$ T cells), M1 macrophages (CD206$^-$ macrophages), dendritic cells (DCs, CD11C$^+$ MHCII$^+$ DCs), and effector DCs (CD86$^+$ DCs). Tumor immunosuppression-related cells included regulatory T cells (Tregs, FOXP3$^+$ CD25$^+$ CD4$^+$ T cells), M2 macrophages (CD206$^+$ macrophages), and myeloid-derived suppressor cells (MDSCs, Gr-1$^+$ CD11B$^+$ MDSCs). In addition, tumor cells (CD45$^-$ Epcam$^+$ cells) and stromal cells (CD45$^-$ Epcam$^-$ cells) were also included. The cells were stained according to a previously described protocol for flow cytometry[22]. Flow cytometry was performed with SONY ID7000. The fluorochrome-conjugated anti-mouse antibodies used in the present study are listed, and the gating strategy and staining panels are shown in Figure 4A.

Tissue section staining

Tumor tissue sections were stained with hematoxylin and eosin (HE), immunohistochemistry (IHC), or immunofluorescence (IF) using a previously described protocol[22]. Masson staining was performed using a trichrome stain kit (Sigma-Aldrich). Average integrated optical density (IOD), fluorescence intensities, and collagen density (Masson staining) in five randomly selected areas for each group were calculated using FIJI ImageJ software (https://imagej.net/software/fiji/).

CCK-8 assay

We performed a CCK-8 assay to measure the effect of BiTP on TGF-β-mediated chemoresistance in PDAC cells. Approximately 3×10^3 viable HPDE6-C7, CFPAC-1, ASPC-1, and KPC cells were seeded in 96-well plates. After overnight culture, 10 ng/ml TGF-β1, 10^5 pM BiTP, or hIgG were added to the plates according to experimental design, and the cells were then treated with serial dilutions of gemcitabine and nab-paclitaxel. After 3 days of incubation, CCK-8 reagent (Dojindo, Japan) was added to the plates for incubation at 37°C for 1 h, and absorbance values were measured at 450 nm using a microplate reader.

Transwell migration and Matrigel invasion assays

Transwell migration and Matrigel invasion assays were performed using 8.0 μm pore size inserts. CFPAC-1 and KPC cells were treated with 10 ng/ml TGF-β1, 10^5 pM BiTP or hIgG for 96 h. Untreated cells were employed as the negative control. 1×10^4 CFPAC-1 and KPC cells were suspended in 200 μl DMEM and seeded in the upper chambers. The lower chambers were filled with 750 μl DMEM containing 20% FBS. Migratory CFPAC-1 and KPC cells were stained with crystal violet solution after incubating for 12 or 18 h. In addition, for invasion Matrigel invasion assay, upper chambers were coated with Matrigel (BD, 354248) and incubated at 37°C for 2 h before seeding cells, and the rest of the steps were completely identical.

Western blot analysis

Approximately 1×10^5 CFPAC-1 and KPC cells were inoculated in 6-well plates. After overnight incubation, 10 ng/ml TGF-β1, 10^5 pM BiTP, anti-PD-L1 antibody, or hIgG were added to the plates according to the experimental design. Cells were then treated with serial dilutions of gemcitabine and albumin-bound paclitaxel. After 5 days of incubation, cells were lysed in RIPA lysis buffer. After sonication at 12 000*g* at 4°C and centrifugation for 15 min, the supernatant was collected. The rest of the procedure was carried out as described previously[22]. The antibodies used in the present study are listed in Supplementary Table 1 (Supplemental Digital Content 1, http://links.lww.com/JS9/C71).

Bulk RNA-seq assay

The bulk RNA-seq assay was conducted by Wuhan Seqhealth (Wuhan Seqhealth Co., Ltd, China) following previously established procedures. We utilized k-means clustering to identify the set of highly expressed genes within each group. Subsequently, GO and KEGG enrichment analyses were carried out using the ClusterGVis package (Jun Zhang (2022), ClusterGVis: One-step to Cluster and Visualize Gene Expression Matrix, https://github.com/junjunlab/ClusterGVis).

Statistical analysis

Data are presented as mean ± standard deviation (SD). Statistical analysis was performed using Student's *t*-test and one-way analysis of variance with GraphPad Prism 9.0 software. Differences were considered statistically significant at $P<0.05$.

Results

Innovatively developed BiTP can simultaneously/dually target both PD-L1 and TGF-β

BiTP was developed based on Check-BODY technology, and it simultaneously dual-targets PD-L1 and TGF-β[18]. BiTP has a modified Fc of human IgG1, with the removal of the binding of FcγRs. The VLm and VHm are the domains of anti-PD-L1, whereas the VHs and VLs are the domains of anti-TGF-β (Fig. 1A).

We first examined the binding affinity of BiTP. As shown in Figure 1B, both BiTP and the anti-PD-L1 antibody were able to bind to human and mouse PD-L1 antigens. As shown in Figure 1C, the binding of human or mouse PD-L1 and PD-1 was competed by BiTP and the anti-PD-L1 antibody. As shown in Figure 1D, both BiTP and the anti-TGF-β antibody bound to TGF-β1/2/3. As shown in Figure 1E, the binding of TGF-β1/2/3 and TGFβRII was competed by BiTP and the anti-TGF-β antibody. These results suggest that BiTP bound to PD-L1 and TGF-β1/2/3 was similar than anti-PD-L1 and anti-TGF-β, and BiTP could almost completely inhibit the binding of PD-L1 to PD-1 and TGF-β1/2/3 to TGF-β1/2/3R *in vitro*.

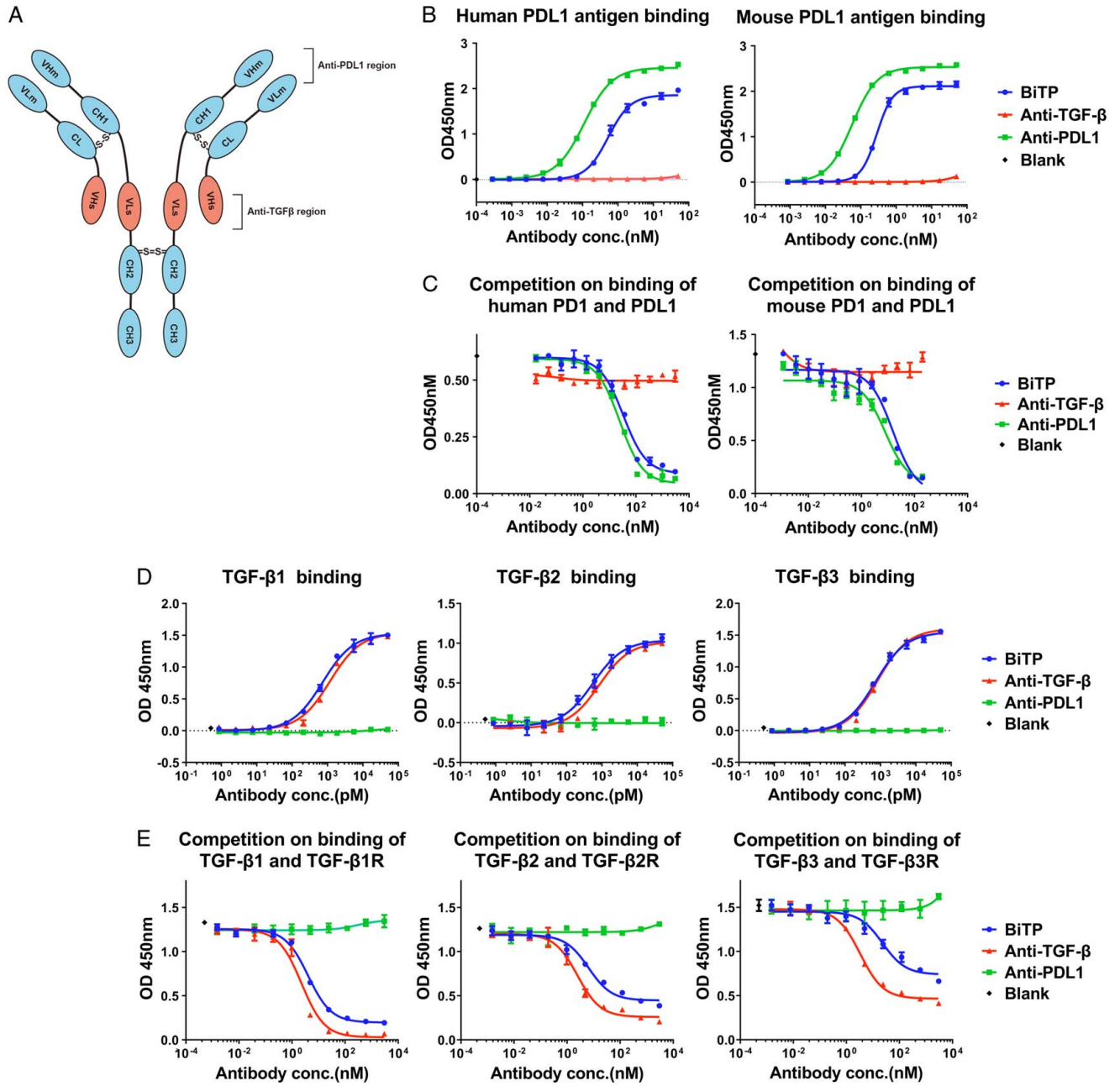

Figure 1. Structure, binding affinity, and competition of BiTP. (A) The structure of BiTP was developed based on Check-BODY technology and targeting PD-L1 and TGF-β. (B, C) The binding affinity and competitive inhibition capability of PD-L1 were evaluated with ELISA (enzyme-linked immunosorbent assays). The EC_{50} (concentration for 50% of maximal effect) values of BiTP and the anti-PD-L1 antibody binding to human PD-L1 were 0.53 and 0.11 nM, respectively, and to mouse PD-L1 were 0.28 and 0.06 nM, respectively. The IC_{50} (the half maximal inhibitory concentration) values of the competition of BiTP and the anti-PD-L1 antibody to human PD-1/PD-L1 were 33.4 and 24.4 nM, respectively, and to mouse PD-1/PD-L1 were 15.4 and 7.9 nM, respectively. (D, E) The binding affinity and competitive inhibition capability to TGF-β1/2/3 were evaluated by ELISA. The EC_{50} values of BiTP binding to TGF-β1/2/3 were 0.73, 0.56, and 0.72 nM, respectively, and of the anti-TGF-β antibody binding to TGF-β1/2/3 were 1.16, 0.84, and 0.82 nM, respectively. The IC_{50} values of the competition of BiTP for the binding of TGF-β1/2/3 to TGFB-β1/2/3R were 4.03, 6.36, and 22.89 nM, respectively, and of the anti-TGF-β antibody were 2.26, 2.45, and 3.32 nM, respectively. BiTP, anti-PD-L1/TGF-β antibody; OD, optical density; PD-L1, programmed cell death 1 ligand 1; TGF-β, transforming growth factor-β.

BiTP enhances the antitumor activity of chemotherapy in orthotopic PDAC mouse models

Pathological features of human PDAC such as fibrosis and inflammation of the TME, exclusion of infiltrating effector T cells, and a poor response to ICI therapy alone can be characteristically replicated in the KPC model[23–25]. We therefore evaluated the antitumor activity of BiTP plus chemotherapy in a murine PDAC orthotopic implantation model (KPC). One week after tumor cell inoculation, the tumors diameter reached around 5 mm (BR status). The mice were randomly grouped and treated with ICI (anti-PD-L1, BiTP) alone, chemotherapy alone, or ICI combination chemotherapy (Fig. 2A, B). ICI therapy alone was not effective against KPC tumors. Compared with ICI

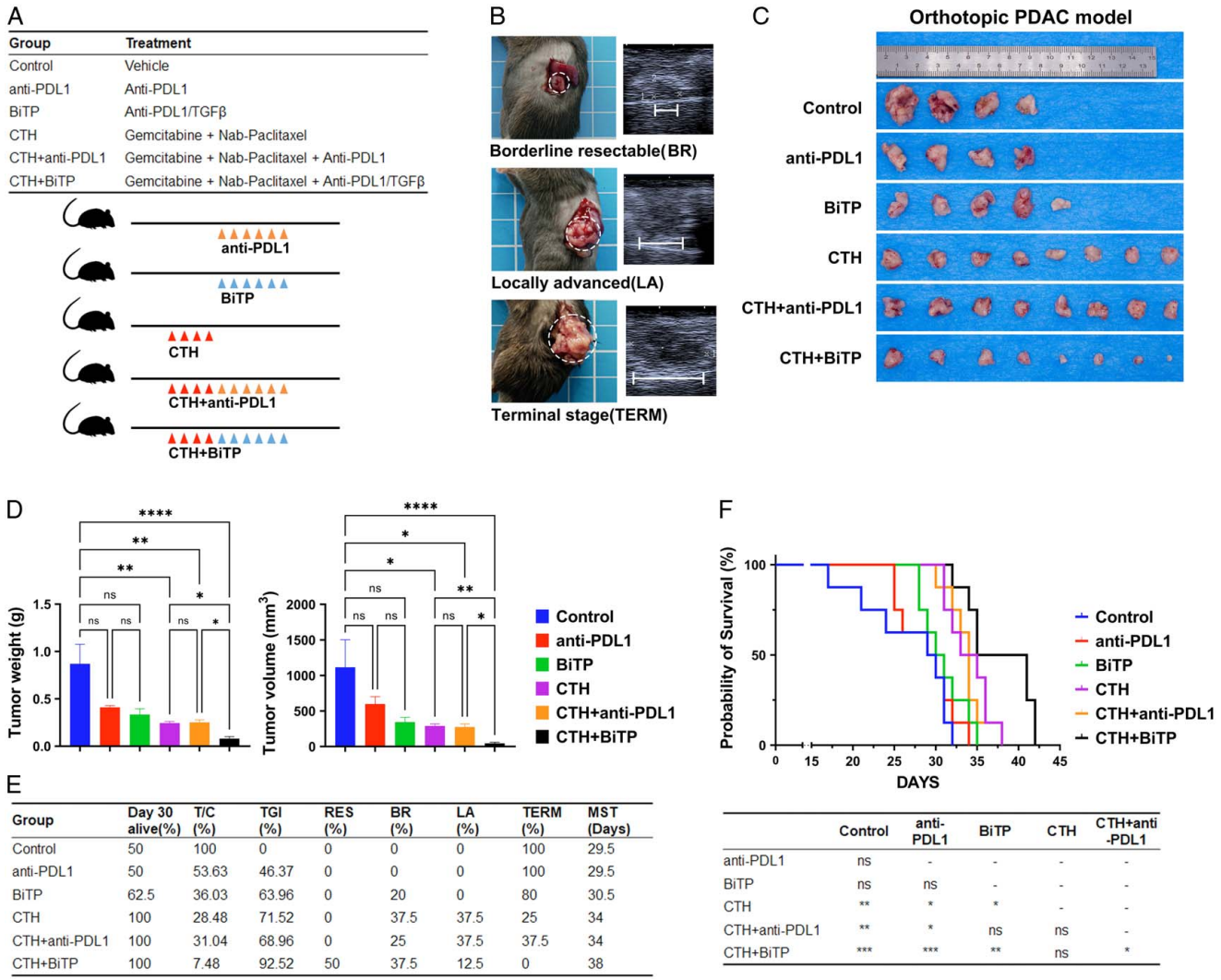

E

Group	Day 30 alive(%)	T/C (%)	TGI (%)	RES (%)	BR (%)	LA (%)	TERM (%)	MST (Days)
Control	50	100	0	0	0	0	100	29.5
anti-PDL1	50	53.63	46.37	0	0	0	100	29.5
BiTP	62.5	36.03	63.96	0	20	0	80	30.5
CTH	100	28.48	71.52	0	37.5	37.5	25	34
CTH+anti-PDL1	100	31.04	68.96	0	25	37.5	37.5	34
CTH+BiTP	100	7.48	92.52	50	37.5	12.5	0	38

	Control	anti-PDL1	BiTP	CTH	CTH+anti-PDL1
anti-PDL1	ns	-	-	-	-
BiTP	ns	ns	-	-	-
CTH	**	*	*	-	-
CTH+anti-PDL1	**	*	ns	ns	-
CTH+BiTP	***	***	**	ns	*

Figure 2. Antitumor activity of BiTP combinatorial chemotherapy in orthotopic PDAC models. (A) Treatment plan and schedules. (B) Schematic diagram of the KPC model. The approximate time frame of mouse tumor progression to borderline resectable (BR), locally advanced (LA), and terminal (TERM) are days 7, 14, and 21, respectively. (C) Representative tumor images of orthotopic PDAC mice receiving different therapies. (D) Tumor weights and volumes on day 30. (E) The table included the survival rate (%), tumor proliferation (T/C, %), tumor growth inhibition (TGI, %), and resectability status of orthotopic PDAC mice receiving different therapies on day 30, and the median survival time (MST) in survival assays. (F) Kaplan–Meier plot survival curve and pairwise comparison results of orthotopic PDAC mice receiving different therapies in survival assays. Data presented in the graphs represent mean ± standard deviation (SD) (****$P < 0.0001$; ***$P < 0.001$; **$P < 0.01$; *$P < 0.05$; ns $P > 0.05$). BiTP, anti-PD-L1/TGF-β antibody; CTH, chemotherapy; PDAC, pancreatic ductal adenocarcinoma; PD-L1, programmed cell death 1 ligand 1.

monotherapy, the inhibitory effect of chemotherapy was evident. Compared with the other five groups, BiTP combination therapy with chemotherapy showed significantly delayed tumor growth (TGI = 92.52%) (Fig. 2C–E). Based on decisions about the resectability status (Table 1), 75% of BiTP plus gemcitabine and nab-paclitaxel-treated tumors were still BR on day 30 (Fig. 2E). Survival assays showed that BiTP plus chemotherapy also slowed the most significant prolongation of survival (Fig. 2F). Aside from these findings, we did not observe any noticeable toxicity or weight loss in mice that received antibody treatment compared to the vehicle or chemotherapy-alone group. No visible damage was detected in the liver and kidneys, and there were no evident pathological changes in the liver sections (Supplementary Fig. S1, Supplemental Digital Content 1, http://links.lww.com/JS9/C71). These results suggest that BiTP is safe and well-tolerated.

Preclinical assessment of neoadjuvant BiTP combinatorial chemotherapy for the treatment of PDAC

Curative resection remains the most critical factor in determining outcomes and is the only possible cure for patients with PDAC. We simulated two common clinical treatment strategies, adjuvant therapy (chemotherapy ± ICI therapy after surgery) and neoadjuvant therapy (surgery after chemotherapy ± ICI therapy) by performing tumor resection (Fig. 3A, B). Neoadjuvant chemoimmunotherapy could completely suppress tumor growth during the treatment period ($P > 0.05$) (Fig. 3J, K). Compared with those in chemotherapy alone, a high BR rate (66.7% vs. 91.7%) and low OM (20% vs. 0%) were obtained in the neoadjuvant chemoimmunotherapy group (Fig. 3G).

A

Group	Treatment
SRG	Surgery alone (Day 7)
SRG+AC	Surgery (Day 7) + Adjuvant Chemotherapy
SRG+ACI	Surgery (Day 7) + Adjuvant Chemotherapy-Immunotherapy (BiTP)
NAT Control	Vehicle +Surgery (Day 24)
NAC+SRG	Neo-adjuvant Chemotherapy + Surgery (Day 24)
NACI+SRG	Neo-adjuvant Chemotherapy-Immunotherapy (BiTP) + Surgery (Day 24)

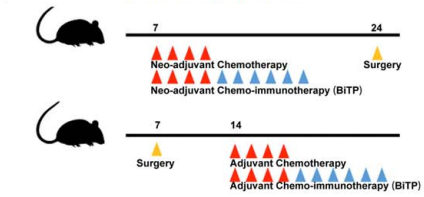

B

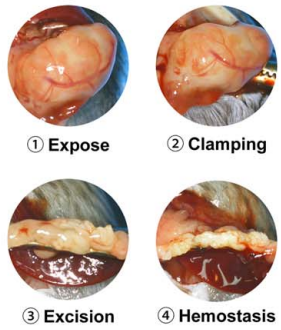

C

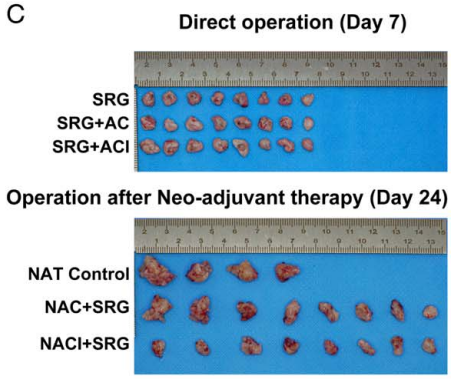

D

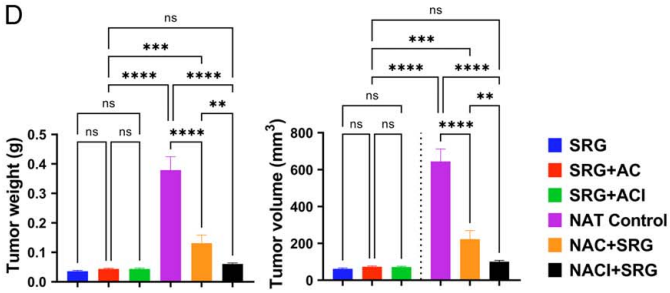

F

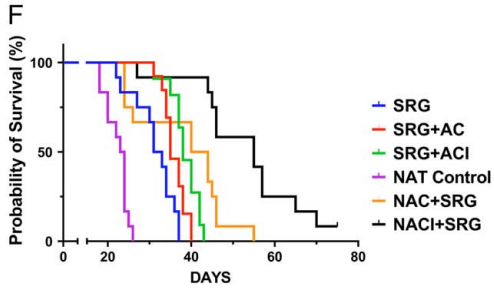

E

Group	BR (%)	LA (%)	TERM (%)	OM (Dead/Total)	MST (Days)
SRG	100	0	0	0/12	32
SRG+AC	100	0	0	0/12	35
SRG+ACI	100	0	0	0/12	38
NAT Control	0	16.7	83.3	2/2	23.5
NAC+SRG	66.7	16.7	16.7	2/10	42
NACI+SRG	91.7	8.3	0	0/12	55

	SRG	SRG +AC	SRG +ACI	NAT Control	NAC +SRG
SRG+AC	*	-	-	-	-
SRG+ACI	***	*	-	-	-
NAT Control	***	****	****	-	-
NAC+SRG	**	*	*	***	-
NACI+SRG	****	****	****	****	*

G

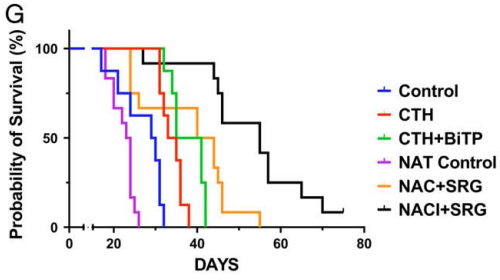

	Control	CTH	CTH +BiTP	NAT Control	NAC +SRG
CTH	**	-	-	-	-
CTH+BiTP	***	ns	-	-	-
NAT Control	*	****	****	-	-
NAC+SRG	**	*	ns	***	-
NACI+SRG	****	***	***	****	*

H

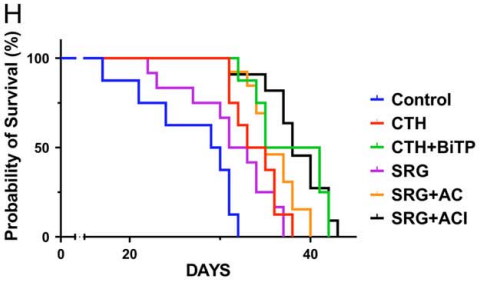

	Control	CTH	CTH +BiTP	SRG	SRG +AC
CTH	**	-	-	-	-
CTH+BiTP	***	ns	-	-	-
SRG	*	ns	*	-	-
SRG+AC	****	ns	ns	*	-
SRG+ACI	****	**	ns	***	*

Figure 3. Preclinical assessment of neoadjuvant BiTP combinatorial chemotherapy for the treatment of PDAC. (A) Treatment plan and schematic diagram of treatment schedules. (B) Schematic diagram of distal pancreatectomy in orthotopic PDAC mice model. (C) Representative images of tumors. (D) Tumor weights and volumes of direct surgery (day 7) and post-neoadjuvant therapy resections (day 24). (E) Table of resectability status (day 24), operative mortality (OM), and median survival time (MST) of orthotopic PDAC mice receiving different therapies. (F–H) Kaplan–Meier plot survival curve and pairwise comparison results of orthotopic PDAC mice receiving different therapies in survival assays. Data presented in the graphs represent mean ± standard deviation (SD). (****$P < 0.0001$; ***$P < 0.001$; **$P < 0.01$; *$P < 0.05$; ns $P > 0.05$). AC, adjuvant chemotherapy; ACI, adjuvant chemo-immunotherapy; BiTP, anti-PD-L1/TGF-β antibody; CTH, chemotherapy; NAC, neo-adjuvant chemotherapy; NACI, neo-adjuvant chemo-immunotherapy; NAT, neo-adjuvant therapy; SRG, surgery.

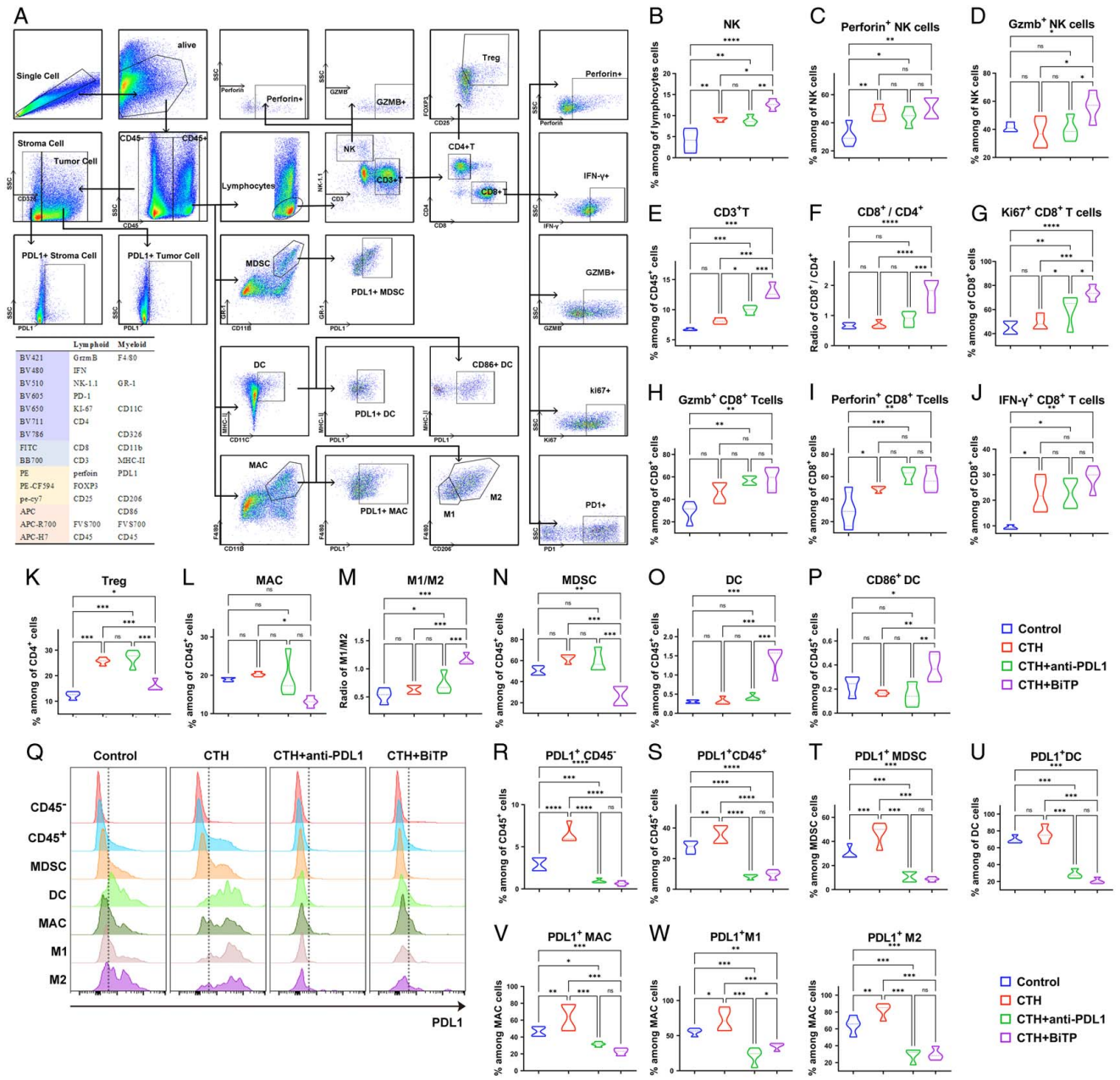

Figure 4. Spectral flow cytometry to explore the mechanism of BiTP synergy with chemotherapy to overcome immune evasion. (A) Gating strategies for T cells, NK cells, DCs, MDSCs, MAC, tumor cells, and stromal cells in spectral flow cytometry assays. (B–K) The quantification of tumor-infiltrating lymphocytes, including NK cells (NK-1.1$^+$ NK cells), effector NK cells (Gzmb$^+$, Perforin$^+$ NK cells), CD8$^+$ T cells (CD3$^+$ CD8$^+$ NK cells)/CD4$^+$ T cells (CD3$^+$ CD4$^+$ T cells), effector CD8$^+$ T cells (Gzmb$^+$, IFN-γ$^+$, Perforin$^+$, and Ki67$^+$ CD8$^+$ T cells), , and Tregs(FOXP3$^+$ CD25$^+$ CD4$^+$ T cells). (L–P) The quantification of tumor-infiltrating myeloid cells, including M1 macrophages (CD206$^-$ macrophages)/M2 macrophages (CD206$^+$ macrophages), MDSCs (Gr-1$^+$ CD11B$^+$ MDSCs), DCs (CD11C$^+$ MHCII$^+$ DCs), and effector DCs (CD86$^+$ DCs). (Q) Flow cytometry assays of PD-L1 expression in different cell subtypes. (R–Y) The quantification of PD-L1$^+$ cells in different cell subtypes. Data presented in the graphs represent mean ± standard deviation (SD) (****$P < 0.0001$; ***$P < 0.001$; **$P < 0.01$; *$P < 0.05$; ns $P > 0.05$). BiTP, anti-PD-L1/TGF-β antibody; CTH, chemotherapy; DC, dendritic cell; MAC, macrophage; MDSC, myeloid-derived suppressor cell; NK cell, natural killer cell; PD-L1, programmed cell death 1 ligand 1; Tregs, regulatory T cells.

Neoadjuvant treatment resulted in a significant survival benefit, with the neoadjuvant chemotherapy combined with BiTP group having the longest median survival time of 55 days, with statistically significant differences from the remaining groups. At the end of neoadjuvant treatment, all mice had indications for resection surgery and had an uneventful postoperative recovery with no surgery-related deaths (Fig. 3E–G). In this preclinical study, neoadjuvant chemotherapy combined with BiTP was highly effective in the junctionally resectable mouse model and was the best treatment regimen to improve the prognosis of the mice.

In the adjuvant therapy group, postoperative chemotherapy alone and postoperative chemoimmunotherapy had a better prognosis than surgery alone ($P < 0.01$ and $P < 0.001$,

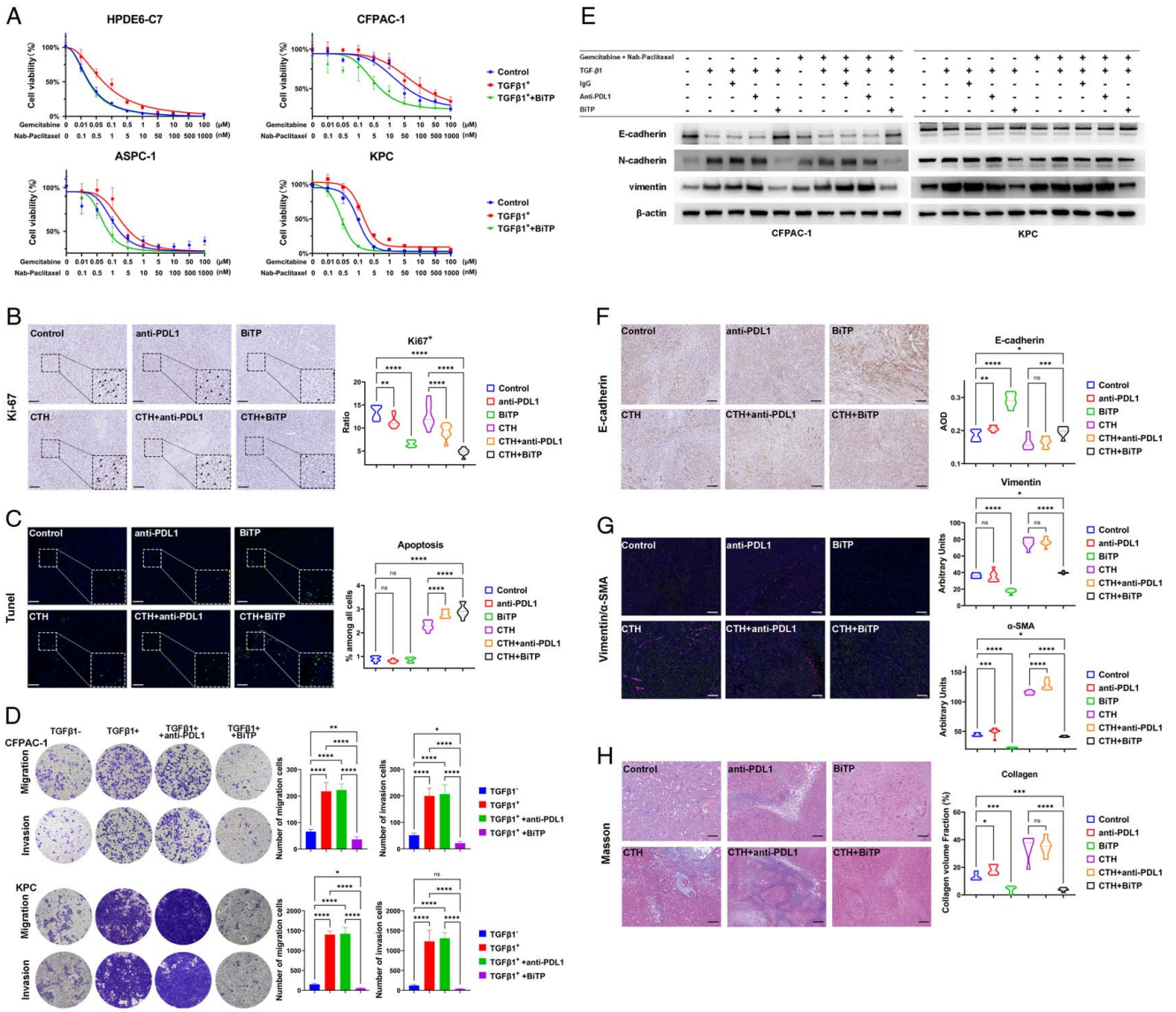

Figure 5. BiTP reverses TGF-β-induced EMT (epithelial–mesenchymal transition) of PDAC (pancreatic ductal adenocarcinoma) cells. (A) CCK-8 (Cell Counting Kit-8) assay to measure the effect of BiTP on TGF-β-mediated chemoresistance in PDAC cells. After 10 ng/ml TGF-β1, 10^5 pM BiTP or hIgG treatment for 24 h. HPDE6-C7, CFPAC-1, ASPC-1, and KPC cells growing in 96-well plates were exposed to serial dilutions of gemcitabine and nab-paclitaxel for 72 h and CCK-8 assays was performed. (B) The representative images of IHC (immunohistochemistry) staining of Ki67 in orthotopic PDAC mice model and statistical graph of the percentage of Ki67-positive cells. (C) The representative images of TUNEL staining for apoptosis (green) and nuclei (DAPI, blue) in orthotopic PDAC mice model and statistical graph of the percentage of apoptosis cells. (D) Transwell assays to measure the effect of BiTP on TGF-β-mediated migration and in PDAC cells. After 10 ng/ml TGF-β1, 10^5 pM BiTP or hIgG treatment for 96 h. 1×10^4 CFPAC-1 and KPC cells were seeded in the upper chambers and Transwell assays were performed. (E) Western blotting assays exploring the chemotherapy-induced EMT and the blocking effect of BiTP. (F) The representative images of IHC staining of E-cadherin in orthotopic PDAC mice model. Statistical graph of the AOD (average optical density) of E-cadherin. (G) The representative images of IF staining of Vimentin (green) and α-SMA (rose red) in orthotopic PDAC mice model. Statistical graph of the arbitrary units of Vimentin and α-SMA. (H) The representative images of Masson staining in orthotopic PDAC mice model. Statistical graph of the percentage of collagen volume fraction (%). Data presented in the graphs represent mean ± standard deviation (SD). (****$P < 0.0001$; ***$P < 0.001$; **$P < 0.01$; *$P < 0.05$; ns $P > 0.05$). BiTP, anti-PD-L1/TGF-β antibody; CTH, chemotherapy; KPC, LSL-Kras(+/G12D);LSL-Trp53(+/R172H);Pdx1-Cre; PDAC, pancreatic ductal adenocarcinoma; PD-L1, programmed cell death 1 ligand 1; TGF-β, transforming growth factor-β.

respectively). The survival of postoperative chemoimmunotherapy was slightly better than that of postoperative chemotherapy alone ($P = 0.038$) (Fig. 3F). Furthermore, compared to the drug-only group (CTH and CTH + BiTP), adjuvant therapy groups (SRG + AC and SRG + ACI) were close in survival, with no significant survival benefit seen (Fig. 3H). In line with our hypothesis, the tumor biology of the mouse model at this stage was also similar to that of the majority of patients with pancreatic cancer at the BR stage in clinical practice, with limited survival benefit with direct surgical resection.

BiTP synergized with chemotherapy by reprogramming TME to overcome immune evasion

In addition to cytotoxicity, chemotherapy affects all components of pancreatic cancer, cellular and noncellular[7,8]. To evaluate the impact of BiTP combinatorial chemotherapy on antitumor

Table 1

Decisions about resectability status in PDAC murine models.

Resectable (RES)	
	Tumor maximum diameter smaller than 4 mm
	No macroscopic metastases[a]
	The tumors had a complete capsule with a smooth surface
	The tumors did not invade the surrounding structures
Borderline resectable (BR)	
	Tumor maximum diameter smaller than 8 mm
	The tumors had a complete capsule with a smooth surface
	The tumors did not invade the surrounding structures
	No macroscopic metastases
Locally advanced (LA)	
	Tumor maximum diameter smaller than 1.2 cm
	The membrane structure was unclear
	The tumor has formed adhesions to the surrounding soft tissue (separable)
Terminal stage (TERM)	
	The tumor has formed dense adhesions to the surrounding soft tissue
	Tumor maximum diameter over 1.2 cm
	Macroscopic metastases
	Mouse showed an emaciated state or cachexia[b]

[a]Macroscopic metastasis foci in the intestine, stomach, liver, kidneys, pelvic, peritoneal, retroperitoneal, or bloody ascites.
[b]Weight loss exceeded 20% of the starting weight.

immunity and reshaping pancreatic TME, we examined the intratumoral infiltration of most studied cell populations in pancreatic cancer through spectral flow cytometry. The density of infiltrating anti-tumorigenic $CD8^+$ or $CD4^+$ T cells was similar in chemotherapy-treated and vehicle groups, but the levels of effector $CD8^+$ T cells (IFN-γ^+, Perforin$^+$ $CD8^+$ T cells) were increased. Combination therapy, especially BiTP, significantly increased the levels of infiltrating anti-tumorigenic cells including NK cells, effector NK cells (Gzmb$^+$, Perforin$^+$ NK cells), effector $CD8^+$ T cells (Gzmb$^+$, IFN-γ^+, Perforin$^+$, and $Ki67^+$ $CD8^+$ T cells), and exhausted CD8 T cells (PD-1^+ $CD8^+$ T cells) (Fig. 4B–J). However, at the same time, after chemotherapy, tumor cells also reshaped the antitumor immunosuppressive microenvironment by promoting the infiltration of immunosuppressive cells (Tregs, M2 macrophages, MDSCs) and suppressing T cell function, which may lead to post-chemotherapy immune evasion. BiTP synergized with chemotherapy to specifically reduce the levels of M2 macrophages, MDSCs, and Tregs in the TME after chemotherapy reversed the remodeling of the immunosuppressive TME by cancer cells and to overcome immune evasion (Fig. 4K–N). The density of DCs and their effect on BiTP-treated tumors (alone or in combination) specifically increased (Fig. 4O, P). IF staining was conducted using tumor samples and showed the same trend (Supplementary Fig. S2, Supplemental Digital Content 1, http://links.lww.com/JS9/C71). After chemotherapy, the expression of PD-L1 on the surface of immunosuppressive cells in tissues increased, and the combined application of BiTP or anti-PD-L1 significantly antagonized the expression of PD-L1 in TME (Fig. 4Q–X).

BiTP reverses the chemotherapy resistance, migration and invasion, epithelial–mesenchymal transition (EMT) of PDAC cells and cancer-associated fibroblasts (CAFs) activation in TME

Chemotherapy resistance, recurrence, and metastasis are important factors that contribute to poor prognosis of PDAC. TGF-β enhanced the chemoresistance and migration capability of cancer cells by inducing EMT. BiTP specifically blocked the TGF-β-induced chemoresistance ability of PDAC cells (Fig. 5A). Compared with the control group, the BiTP antagonized both endogenous and exogenous TGFβ, and the combined treatment significantly enhanced the cytotoxicity of chemotherapy drugs to malignant tumor cells (CFPAC-1, ASPC-1, and KPC). The IC_{50} values in each group are listed in Supplementary Table 4 (Supplemental Digital Content 1, http://links.lww.com/JS9/C71). IHC staining of Ki67 and TUNEL staining was conducted using tumor samples and showed that BiTP synergy with chemotherapy to inhibit tumor proliferation and promote tumor apoptosis (Fig. 5B, C).

We continue to determine if BiTP impacts EMT in PDAC cells. BiTP also specifically blocked EMT in PDAC cells, thereby restraining cellular mobility in terms of migration and invasion, upregulating the level of an epithelial marker (E-cadherin), and downregulating the levels of mesenchymal markers (N-cadherin and Vimentin). At the same time, the anti-PD-L1 antibody did not affect EMT in cancer cells (Fig. 5D, E). Moreover, we investigated the influence of BiTP treatment on EMT. IHC and IF staining results showed that BiTP upregulated E-cadherin expression and downregulated Vimentin expression (Fig. 5F, G).

A significant component of the stroma is CAFs that are tumor-promoting cells that assist tumor progression. Collagen and α-SMA are classic markers of CAFs. Masson staining (Collagen) and IF (α-SMA) were conducted using tumor samples (Fig. 5G, H). In contrast to the vehicle, chemotherapy, and anti-PD-L1 therapy, BiTP significantly reduced α-SMA expression and collagen deposition.

BiTP, in synergy with chemotherapy, engages multiple signaling pathways

To explore the mechanisms of antitumor activity of BiTP synergizes with chemotherapy, we performed a bulk RNA sequencing using tumor tissues of orthotopic tumor transplantation murine (Control, Chemotherapy, Chemotherapy + anti-PD-L1, Chemotherapy + BiTP). KEGG and GO enrichment analyses were performed (Supplementary Fig. S3, Supplemental Digital Content 1, http://links.lww.com/JS9/C71). Enrichment analyses revealed that BiTP synergizes with chemotherapy (Cluster 4, C4), leading to the specific upregulation of multiple immune-related pathways. These pathways encompass the activation of the immune response, complement activation, lymphocyte-mediated immunity, positive regulation of lymphocyte activation, B cell activation, B cell-mediated immunity, and others. BiTP synergizes with chemotherapy to effectively inhibit the activation of various

chemotherapy-induced pathways and induce altered epigenetic modifications (Cluster 1, C1). These include, but are not limited to, the Wnt signaling pathway, Notch signaling pathway, AMPK signaling pathway, histone modification, protein acetylation, histone acetylation, RNA splicing, and others.

Discussion

Neoadjuvant therapy should be considered for patients with BR diseases, followed by restaging and resection in those without disease progression prevention. Although preoperative treatment can be effective and well tolerated in patients with BR pancreatic adenocarcinomas[26,27], R0 resections were only achieved in 31–35% of patients with BR diseases following the completion of neoadjuvant therapy[28,29]. Aiming to improve R0 resection rate and overall survival of neoadjuvant therapy, we designed a novel surgical model of PDAC mice model and combined BiTP with chemotherapy as neoadjuvant chemoimmunotherapy. The encouraging results of our preclinical study suggest that BiTP combined with chemotherapy might be a promising drug combination for PDAC neoadjuvant therapy.

In recent years, cancer immunotherapy has been transformed by ICIs. Treatment with PD-1/PD-L1 or CTLA-4 ICIs can result in long-term tumor responses in patients with advanced solid malignancies across a wide range of tumor types[30]. However, single-agent ICIs have also met their Waterloo in pancreatic cancer immunotherapy, with disappointing early trial results[11–14]. The failure of single-agent immune checkpoint blockade is likely caused by a combination of mechanisms leading to immune evasion.

Unlike breast cancer studies[18], where BiTP monotherapy exhibits extremely limited therapeutic and immune-activating effects on PDAC tumors. Although ICIs therapy used alone show poor effectiveness in the treatment of PDAC. ICIs combinatorial chemotherapy could improve the therapeutic effect of antitumor therapy. Contrastingly, BiTP combinatorial chemotherapy showed significantly delayed tumor growth (TGI = 92.52%) and significant survival benefit compared with other treatment groups.

Neoadjuvant chemotherapy has dramatically improved the prognosis of patients with pancreatic cancer through direct cytotoxicity and restoration of local antitumor immune response[31]. Evidence suggests that neoadjuvant therapy restores the local antitumor immune response, enhances systemic immunity, and eradicates residual metastasis more effectively in addition to being directly cytotoxic to cancer cells[6,7,9,10].

To enable investigations on disease progression as well as neoadjuvant therapies, we developed resectable PDAC mice. Based on the progression rule of the tumor model and the evaluation index of tumor resectability widely adopted in clinics, we established a system for evaluating the resectability of pancreatic tumors in mice. One week after establishing the orthotopic pancreatic tail PDAC model, the tumor diameter exceeded over 4 mm, the capsule was still intact, and no apparent metastasis or invasion of surrounding organs had occurred. We defined the tumor at this stage as BR. In this case, most tumors can be successfully removed by surgery. Based on this set of criteria and surgical excision techniques, we evaluated postoperative (adjuvant) and preoperative (neoadjuvant) therapies in PDAC, and they included BiTP plus chemotherapy for postoperative chemoimmunotherapy and preoperative chemoimmunotherapy. Neoadjuvant chemoimmunotherapy completely suppressed tumor growth during treatment. Compared with those in chemotherapy alone, a high BR rate (66.7% vs. 91.7%) and low OM (20% vs. 0%) were obtained in the neoadjuvant chemoimmunotherapy group. If the time to surgery after neoadjuvant chemoimmunotherapy is extended to day 30, 50% of mouse tumors can even be reduced from the BR to resectable (RES) status. In animal models, similar to that in clinical studies, neoadjuvant chemotherapy resulted in survival benefits in PDAC mice. Adjuvant and neoadjuvant chemoimmunotherapy (BiTP) resulted in survival benefits compared with chemotherapy alone. However, it is worth noting that even in mouse models, surgery remains a mandatory option for further prolonging survival.

Pancreatic cancer is typically a 'cold' tumor with low immunogenicity. In theoretical terms, effective immunotherapeutic strategies are required to activate and maintain the antitumor immune cycle including enhancing antigenicity and antigen presentation, enhancing T cell function and reversing immune escape, and T cell suppression[32]. It is well known that chemotherapy can kill tumor cells through cytotoxicity, release a large amount of tumor cell antigen epitopes, and start the antitumor immune cycle. The dual-target inhibition of BiTP can antagonize PD-L1, effectively enhance T cells or NK cells function, and at the same time antagonize TGF-β-related immunosuppressive effects, thereby enhancing and maintaining the antitumor immune cycle. Therefore, chemotherapy combined with BiTP theoretically has a theoretical basis for synergistically activating and maintaining antitumor immune responses.

There are both tumor-promoting and antitumour effects generated by TGF-β. TGF-β suppresses epithelial cell proliferation initially, but promotes stromal support for cancer and immunosuppression during its later stages. As for immunosuppression, TGF-β induces Treg cells and directly represses several functions of effector T cells[33]. As a result, inhibition of TGF-β enhanced the effects of ICIs in several different mouse models, including the KPC model of PDAC[34–37]. TGF-β activation is also closely associated with PD-L1 resistance in cancer patients[14]. Dual blockade of TGF-β and PD-L1 was feasible in cancer treatment[38–40]. BiTP showed significant advantages over the anti-PD-L1 antibody in PDAC ICI combinatorial chemotherapy. DCs, as the most potent specific antigen-presenting cells in the body, play a vital role in initiating and regulating immune response[41]. The density of DCs and the number of effector DC cells were significantly upregulated through anti-TGF-β therapy. TGF-β could also regulate the functions of multiple immune cells, such as reducing the cytotoxicity of T cells and NK cells and inducing the differentiation of Tregs and macrophages. BiTP synergized with chemotherapy, specifically reducing the levels of M2 macrophages, MDSCs, and Tregs in the TME, overcoming post-chemotherapy immune evasion. Consistent with the results of other studies[42–44], the anti-TGF-β moiety of the BiTP reversed TGF-β-induced EMT of PDAC cells, which led to inhibited EMT-associated tumor cell invasion and metastasis in our study.

PDAC is classically surrounded by desmoplastic stroma composed of CAFs and ECM. The stroma provides a dense mechanical barrier against immune cell trafficking and vascularization, which is a potential cause of the rapid recurrence and progression of pancreatic cancer after chemotherapy[45]. Fibroblasts are typically cells that promote steady-state wound repair, and our study showed that post-chemotherapy pancreatic

tissue injury promoted fibroblast activation and proliferation. Cancer cells can direct and selectively induce the differentiation of surrounding fibroblasts into an inflammatory CAF and myofibroblast CAF phenotype by IL-1 or TGF-β, respectively. IL-6 secreted by inflammatory CAFs then provides a pro-proliferative effect on the tumor, while myofibroblast CAFs are stimulated by TGF-β to produce surrounding stroma[46,47]. In addition, in the research of biomechanics, significant stromal components made PDAC became one of the stiffest malignancies with solid stresses exceeding 10 kPa[48,49]. In a previous study, we observed that high matrix stiffness (10–25 kPa, mainly caused by collagen deposition of CAFs) can directly promote PDAC progression and tumor immunosuppression[50]. Chemotherapy significantly increased the α-SMA expression and collagen deposition in TME (fibroblast activation and matrix proliferation), which could be inhibited explicitly by bispecific antibodies in our research.

Conclusion

In conclusion, we developed a novel therapeutic antibody BiTP, which simultaneously and dually blocks TGF-β and PD-1/PD-L1 pathways. The BiTP synergizes with chemotherapy through reprogramming pancreatic TME to overcome immune evasion post-chemotherapy. Although the therapeutic effect is limited when used alone, BiTP in combination with chemotherapy results in significant tumor downstaging and survival benefits in neoadjuvant chemoimmunotherapy.

Ethical approval

Not applicable.

Consent

Not applicable.

Sources of funding

This work was supported by the National Natural Science Foundation of China (81772564, 82173196), the Key Research and Development Program of Hubei (2022BCA012) and the Joint Funds for the Innovation of Science and Technology, Fujian Province (2023Y9311).

Author contribution

H.Z., T.Y., J.Z., S.H., and P.Z.: study concept or design; H.Z., J.C., J.B., T.Y., and L.Z.: data collection, data analysis, or interpretation; H.Z., J.C., T.Y., and Q.S.: writing the paper.

Conflicts of interest disclosure

J.Z., S.H., L.Z., and P.Z. were employees of Wuhan YZY Biopharma Co., Ltd.

Research registration unique identifying number (UIN)

Not applicable.

Guarantor

Tao Yin.

Data availability statement

All data used to support the findings of this study is available from the corresponding author upon request.

Provenance and peer review

Submitted without invited.

Acknowledgements

The authors are grateful for the technical support from the Analytical & Testing Center and Medical Sub-Center of Huazhong University of Science & Technology.

References

[1] Rahib L, Smith BD, Aizenberg R, *et al*. Projecting cancer incidence and deaths to 2030: the unexpected burden of thyroid, liver, and pancreas cancers in the United States. Cancer Res 2014;74:2913–21.
[2] Kunzmann V, Siveke JT, Algul H, *et al*. Nab-paclitaxel plus gemcitabine versus nab-paclitaxel plus gemcitabine followed by FOLFIRINOX induction chemotherapy in locally advanced pancreatic cancer (NEOLAP-AIO-PAK-0113): a multicentre, randomised, phase 2 trial. Lancet Gastroenterol Hepatol 2021;6:128–38.
[3] Yamaguchi J, Yokoyama Y, Fujii T, *et al*. Results of a phase II study on the use of neoadjuvant chemotherapy (FOLFIRINOX or GEM/nab-PTX) for borderline-resectable pancreatic cancer (NUPAT-01). Ann Surg 2022; 275:1043–9.
[4] Gillen S, Schuster T, Meyer Zum Buschenfelde C, *et al*. Preoperative/ neoadjuvant therapy in pancreatic cancer: a systematic review and meta-analysis of response and resection percentages. PLoS Med 2010;7: e1000267.
[5] Oettle H, Neuhaus P, Hochhaus A, *et al*. Adjuvant chemotherapy with gemcitabine and long-term outcomes among patients with resected pancreatic cancer: the CONKO-001 randomized trial. JAMA 2013;310: 1473–81.
[6] Hane Y, Tsuchikawa T, Nakamura T, *et al*. Immunological gene signature associated with the tumor microenvironment of pancreatic cancer after neoadjuvant chemotherapy. Pancreas 2020;49:1240–5.
[7] Mota Reyes C, Teller S, Muckenhuber A, *et al*. Neoadjuvant therapy remodels the pancreatic cancer microenvironment via depletion of protumorigenic immune cells. Clin Cancer Res 2020;26:220–31.
[8] Heiduk M, Plesca I, Gluck J, *et al*. Neoadjuvant chemotherapy drives intratumoral T cells toward a proinflammatory profile in pancreatic cancer. JCI Insight 2022;7:e152761.
[9] Gurlevik E, Fleischmann-Mundt B, Brooks J, *et al*. Administration of gemcitabine after pancreatic tumor resection in mice induces an antitumor immune response mediated by natural killer cells. Gastroenterology 2016; 151:338–50.e7.
[10] Liu J, Blake SJ, Yong MC, *et al*. Improved efficacy of neoadjuvant compared to adjuvant immunotherapy to eradicate metastatic disease. Cancer Discov 2016;6:1382–99.
[11] Royal RE, Levy C, Turner K, *et al*. Phase 2 trial of single agent Ipilimumab (anti-CTLA-4) for locally advanced or metastatic pancreatic adenocarcinoma. J Immunother 2010;33:828–33.
[12] Patnaik A, Kang SP, Rasco D, *et al*. Phase I study of pembrolizumab (MK-3475; anti-PD-1 monoclonal antibody) in patients with advanced solid tumors. Clin Cancer Res 2015;21:4286–93.
[13] Herbst RS, Soria JC, Kowanetz M, *et al*. Predictive correlates of response to the anti-PD-L1 antibody MPDL3280A in cancer patients. Nature 2014;515:563–7.
[14] Brahmer JR, Tykodi SS, Chow LQ, *et al*. Safety and activity of anti-PD-L1 antibody in patients with advanced cancer. N Engl J Med 2012;366: 2455–65.

[15] Chen J, Gingold JA, Su X. Immunomodulatory TGF-beta signaling in hepatocellular carcinoma. Trends Mol Med 2019;25:1010–23.
[16] Oshimori N, Oristian D, Fuchs E. TGF-beta promotes heterogeneity and drug resistance in squamous cell carcinoma. Cell 2015;160:963–76.
[17] Jakowlew SB. Transforming growth factor-beta in cancer and metastasis. Cancer Metastasis Rev 2006;25:435–57.
[18] Yi M, Wu Y, Niu M, *et al*. Anti-TGF-beta/PD-L1 bispecific antibody promotes T cell infiltration and exhibits enhanced antitumor activity in triple-negative breast cancer. J Immunother Cancer 2022;10:e005543.
[19] Yi M, Niu M, Zhang J, *et al*. Combine and conquer: manganese synergizing anti-TGF-beta/PD-L1 bispecific antibody YM101 to overcome immunotherapy resistance in non-inflamed cancers. J Hematol Oncol 2021;14:146.
[20] Yi M, Zhang J, Li A, *et al*. The construction, expression, and enhanced anti-tumor activity of YM101: a bispecific antibody simultaneously targeting TGF-beta and PD-L1. J Hematol Oncol 2021;14:27.
[21] Kilkenny C, Browne WJ, Cuthill IC, *et al*. Improving bioscience research reporting: the ARRIVE guidelines for reporting animal research. PLoS Biol 2010;8:e1000412.
[22] Wu S, Zhang H, Gao C, *et al*. Hyperglycemia enhances immunosuppression and aerobic glycolysis of pancreatic cancer through upregulating Bmi1–UPF1–HK2 pathway. Cell Mol Gastroenterol Hepatol 2022;14:1146–65.
[23] Luo Y, Li Z, Kong Y, *et al*. KRAS mutant-driven SUMOylation controls extracellular vesicle transmission to trigger lymphangiogenesis in pancreatic cancer. J Clin Invest 2022;132:e157644.
[24] Peran I, Dakshanamurthy S, McCoy MD, *et al*. Cadherin 11 promotes immunosuppression and extracellular matrix deposition to support growth of pancreatic tumors and resistance to gemcitabine in mice. Gastroenterology 2021;160:1359–72.e13.
[25] Ma Y, Li J, Wang H, *et al*. Combination of PD-1 inhibitor and OX40 agonist induces tumor rejection and immune memory in mouse models of pancreatic cancer. Gastroenterology 2020;159:306–19.e12.
[26] Katz MH, Shi Q, Ahmad SA, *et al*. Preoperative modified FOLFIRINOX treatment followed by capecitabine-based chemoradiation for borderline resectable pancreatic cancer: alliance for clinical trials in oncology trial A021101. JAMA Surg 2016;151:e161137.
[27] Esnaola NF, Chaudhary UB, O'Brien P, *et al*. Phase 2 trial of induction gemcitabine, oxaliplatin, and cetuximab followed by selective capecitabine-based chemoradiation in patients with borderline resectable or unresectable locally advanced pancreatic cancer. Int J Radiat Oncol Biol Phys 2014;88:837–44.
[28] Stokes JB, Nolan NJ, Stelow EB, *et al*. Preoperative capecitabine and concurrent radiation for borderline resectable pancreatic cancer. Ann Surg Oncol 2011;18:619–27.
[29] McClaine RJ, Lowy AM, Sussman JJ, *et al*. Neoadjuvant therapy may lead to successful surgical resection and improved survival in patients with borderline resectable pancreatic cancer. HPB (Oxford) 2010;12:73–9.
[30] Hamid O, Chiappori AA, Thompson JA, *et al*. First-in-human study of an OX40 (ivuxolimab) and 4-1BB (utomilumab) agonistic antibody combination in patients with advanced solid tumors. J Immunother Cancer 2022;10:e005471.
[31] Ghanim B, Klikovits T, Hoda MA, *et al*. Ki67 index is an independent prognostic factor in epithelioid but not in non-epithelioid malignant pleural mesothelioma: a multicenter study. Br J Cancer 2015;112:783–92.
[32] Chen DS, Mellman I. Oncology meets immunology: the cancer-immunity cycle. Immunity 2013;39:1–10.
[33] Principe DR, Doll JA, Bauer J, *et al*. TGF-beta: duality of function between tumor prevention and carcinogenesis. J Natl Cancer Inst 2014;106:djt369.
[34] Tauriello DVF, Palomo-Ponce S, Stork D, *et al*. TGFbeta drives immune evasion in genetically reconstituted colon cancer metastasis. Nature 2018;554:538–43.
[35] Principe DR, Park A, Dorman MJ, *et al*. TGFbeta blockade augments PD-1 inhibition to promote T-cell-mediated regression of pancreatic cancer. Mol Cancer Ther 2019;18:613–20.
[36] Mariathasan S, Turley SJ, Nickles D, *et al*. TGFbeta attenuates tumour response to PD-L1 blockade by contributing to exclusion of T cells. Nature 2018;554:544–8.
[37] Metropulos AE, Munshi HG, Principe DR. The difficulty in translating the preclinical success of combined TGFbeta and immune checkpoint inhibition to clinical trial. EBioMedicine 2022;86:104380.
[38] Tan B, Khattak A, Felip E, *et al*. Bintrafusp Alfa, a Bifunctional Fusion Protein Targeting TGF-beta and PD-L1, in Patients with Esophageal Adenocarcinoma: Results from a Phase 1 Cohort. Target Oncol 2021;16:435–46.
[39] Barlesi F, Isambert N, Felip E, *et al*. Bintrafusp alfa, a bifunctional fusion protein targeting TGF-beta and PD-L1, in patients with non-small cell lung cancer resistant or refractory to immune checkpoint inhibitors. Oncologist 2023;28:258–67.
[40] Lan Y, Zhang D, Xu C, *et al*. Enhanced preclinical antitumor activity of M7824, a bifunctional fusion protein simultaneously targeting PD-L1 and TGF-beta. Sci Transl Med 2018;10:eaan5488.
[41] Huang WZ, Hu WH, Wang Y, *et al*. A mathematical modelling of initiation of dendritic cells-induced T cell immune response. Int J Biol Sci 2019;15:1396–403.
[42] Principe DR, DeCant B, Mascarinas E, *et al*. TGFbeta signaling in the pancreatic tumor microenvironment promotes fibrosis and immune evasion to facilitate tumorigenesis. Cancer Res 2016;76:2525–39.
[43] Xu J, Lamouille S, Derynck R. TGF-beta-induced epithelial to mesenchymal transition. Cell Res 2009;19:156–72.
[44] Siegel PM, Massague J. Cytostatic and apoptotic actions of TGF-beta in homeostasis and cancer. Nat Rev Cancer 2003;3:807–21.
[45] Provenzano PP, Cuevas C, Chang AE, *et al*. Enzymatic targeting of the stroma ablates physical barriers to treatment of pancreatic ductal adenocarcinoma. Cancer Cell 2012;21:418–29.
[46] Elyada E, Bolisetty M, Laise P, *et al*. Cross-species single-cell analysis of pancreatic ductal adenocarcinoma reveals antigen-presenting cancer-associated fibroblasts. Cancer Discov 2019;9:1102–23.
[47] Biffi G, Oni TE, Spielman B, *et al*. IL1-induced JAK/STAT signaling is antagonized by TGFbeta to shape CAF heterogeneity in pancreatic ductal adenocarcinoma. Cancer Discov 2019;9:282–301.
[48] Rice AJ, Cortes E, Lachowski D, *et al*. Matrix stiffness induces epithelial–mesenchymal transition and promotes chemoresistance in pancreatic cancer cells. Oncogenesis 2017;6:e352.
[49] Laklai H, Miroshnikova YA, Pickup MW, *et al*. Genotype tunes pancreatic ductal adenocarcinoma tissue tension to induce matricellular fibrosis and tumor progression. Nat Med 2016;22:497–505.
[50] Zhang H, Chen J, Hu X, *et al*. Adjustable extracellular matrix rigidity tumor model for studying stiffness dependent pancreatic ductal adenocarcinomas progression and tumor immunosuppression. Bioeng Transl Med 2023;8:e10518.